Time-Dependent Solutions of the Mild-Slope Wave Equation

James T. Kirby, Changhoon Lee [1] and Chris Rasmussen [2]

Abstract

Time dependent forms of the mild-slope wave equation are applied to the propagation of regular and irregular wave trains over variable bathymetry. The model equation of Smith and Sprinks is found to be a robust predictor of irregular waves, if the frequency spread for a single component calculation is not made too large. The model is extended to include forced, low-frequency components, and some preliminary results for bound and free long wave computation are shown.

Introduction

Based on the work of Smith and Sprinks (1975), the mild-slope wave equation for linear waves with a dominant carrier frequency ω and small frequency spread may be written as

$$\tilde{\phi}_{tt} - \nabla_h \cdot (CC_g \nabla_h \tilde{\phi}) + (\omega^2 - k^2 CC_g)\tilde{\phi} = 0 \qquad (1)$$

where $\tilde{\phi}$ is the value of the velocity potential at the mean surface $z = 0$. This equation reduces to Berkhoff's (1972) elliptic equation when the time dependence of purely periodic waves is extracted.

In the past, many solutions of the elliptic problem for open coastal zones have been obtained using a parabolic approximation, which treats the forward-propagating portion of the wave field only. This step has often been taken because of its computational efficiency. The applicability of parabolic approximations is limited, however, to regions without complicated structural boundaries. In particular, complex entrance channels and interiors of harbors are not good candidates for this modelling technique, since the wave field is built up by a number of reflections and re-reflections of waves within the enclosed domains. For these applications, full solutions to the complete boundary-value problem must be found. Progress in obtaining efficient solutions using sophisticated pre-conditioning schemes has been made by Panchang et al (1991).

As an alternative to the elliptic equation approach, several authors (Ito and Tanimoto, 1972; Copeland, 1985; Madsen and Larsen, 1987) have obtained solutions to time-dependent, three-equation models using time-stepping techniques based on equations which are first-order in time. These models are essentially numerical analogs to the more familiar shallow water equations. The model solutions are computed until

---

[1] Center for Applied Coastal Research, Department of Civil Engineering, University of Delaware, Newark, DE 19716

[2] New York District, U.S. Army Corps of Engineers, New York, NY

Kirby

the amplitude envelopes reach a steady state. The final solutions are only valid for purely periodic wave trains, since the three-equation models used are, for the most part, equivalent to the second order model

$$\tilde{\phi}_{tt} - \frac{C}{C_g} \nabla_h \cdot (CC_g \nabla_h \tilde{\phi}) = 0. \tag{2}$$

This model differs from the correct form (1), and is non-dispersive in the sense that modulations of the carrier wave train propagate at the wave phase speed, rather than at the group velocity, as would be required in a correct time-dependent model.

Since the application of time-stepping solutions to the mild-slope equation is a reasonably efficient line of approach, and since it is desirable to provide a model which is valid for unsteady wave trains, it would be advantageous to use a set of model equations which preserves the proper wave group behavior for non-periodic, narrow-banded wave trains. Such a model would be useful in computing effects such as second-order oscillations forced by wave groups.

In section 2, we derive the time-dependent mild-slope equations. In section 3, the dispersiveness of the resulting model is verified by studying wave group propagation over a flat bottom. In section 4 we consider the propagation of linear and weakly nonlinear waves over an elliptic shoal. Section 5 considers two-dimensional propagation of waves over an elliptic shoal using monochromatic and random waves. Finally, in section 6, we discuss the forcing of long wave components at difference frequencies due to non-resonant wave-wave interactions.

Derivation of the time-dependent model equations

The model equations are derived here using Hamilton's variational principle. The Lagrangian for irrotational motion is given by

$$L = -\rho \int_{-h}^{\eta} [\phi_t + \frac{1}{2}(\nabla_h \phi)^2 + \frac{1}{2}(\phi_z)^2 + gz] dz \tag{3}$$

The z dependence is extracted from $\phi(x, y, z, t)$ according to

$$\phi(x, y, z, t) = \tilde{\phi}(x, y, t) f(z) \tag{4}$$

where

$$f(z) = \frac{\cosh k(h + z)}{\cosh kh} \tag{5}$$

From the variational principle the change of the integral of the Lagrangian, L, over all time and space must be equal to zero:

$$\delta \int_t \int_y \int_x L(x, y, t, \phi, \nabla_h \phi, \phi_t, \eta) dx dy dt = 0 \tag{6}$$

Substituting (3) into (6) and retaining the terms to the second order in ϕ and η gives

$$-\rho L = \eta \tilde{\phi}_t + \frac{1}{2} g \eta^2 + \frac{1}{2} \frac{CC_g}{g} (\nabla_h \tilde{\phi})^2 + \frac{1}{2} \frac{(\omega^2 - k^2 CC_g)}{g} (\tilde{\phi})^2 \tag{7}$$

Varying the Lagrangian L with respect to $\tilde{\phi}$ and η gives

$$\eta_t = -\nabla_h \cdot (\frac{CC_g}{g} \nabla_h \tilde{\phi}) + \frac{(\omega^2 - k^2 CC_g)}{g} \tilde{\phi} \tag{8}$$

$$\tilde{\phi}_t = -g\eta \tag{9}$$

Kirby

2

which are the time-dependent mild-slope equations. The surface displacement may be eliminated from (8) and (9) in order to obtain the model equation (1). In this study, we have employed a number of numerical methods fairly interchangeably, including a second-order, centered-time centered-space finite difference approximation for (1), and a fourth-order accurate Adams-Bashforth-Moulton method for (8) and (9). (Use of this latter method was motivated by a parallel effort for the Boussinesq equations, which will be reported separately.)

As in Madsen and Larsen (1987), it is convenient to remove the fast time behavior from the dependent variables by means of the transformation

$$\eta, \tilde{\phi} = (\hat{\eta}, \hat{\phi})e^{-i\omega t} \tag{10}$$

where ω is the frequency used to evaluate the model coefficients. The resulting model equations are

$$\hat{\eta}_t = i\omega\hat{\eta} - \nabla_h \cdot \left(\frac{CC_g}{g}\nabla_h\hat{\phi}\right) + \frac{(\omega^2 - k^2CC_g)}{g}\hat{\phi} \tag{11}$$

$$\hat{\phi}_t = i\omega\hat{\phi} - g\hat{\eta} \tag{12}$$

instead of (8) and (9), and

$$\hat{\phi}_{tt} - 2i\omega\hat{\phi}_t - \nabla_h \cdot (CC_g\nabla_h\hat{\phi}) - k^2CC_g\hat{\phi} = 0 \tag{13}$$

instead of (1). The same set of numerical schemes are also used for the revised model.

Wave group propagation

The basic ability of the model to propagate dispersive linear waves is tested by examining wave group propagation over constant depth. Two numerical experiments were performed. An initial wavelength of $10m$ was specified, with shallow and deep water depths of $0.25m$ and $9m$, respectively. The initial conditions are η and $\tilde{\phi} = 0$. A narrow-banded groupy wavetrain is generated at the boundary according to

$$\tilde{\phi}_x = u_0 \sin(\omega t)\sin(\frac{\omega}{20}t); \qquad t \geq 0 \tag{14}$$

The results shown in figure 1 are water surface elevations plotted at a sequence of twenty time levels spaced one wave period apart. These results were obtained using the Euler Predictor-Corrector method with second-order accurate finite differences (Kirby and Rasmussen, 1991). Two lines are shown on each graph; one following the maximum amplitude of a specific wave group, and the other following a zero crossing of a specific wave. Visually, it appears that in shallow water $C_g \approx C$, and in deep water $C_g \approx C/2$, which shows the validity of the models to predict wave group velocity. Examination of the wave records and computed envelopes using cross-correlation techniques shows that the phase and group velocities are accurately predicted to within 1% for the differencing resolutions used here.

Berkhoff, Booij and Radder shoal experiment

As an example of the application of the models in two-dimensions, we study the focussing of waves by a shoal, using the geometry and experimental parameters given in Berkhoff et al. (1982). It is known from parabolic model computations (Kirby and Dalrymple,
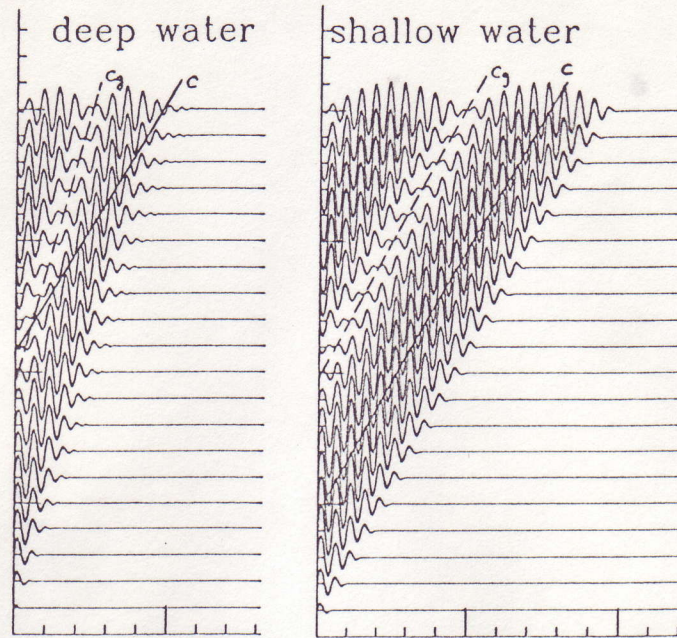
Kirby

3

Figure 1: Propagation of wave groups in deep and shallow water.

1984) that the waves in this example are significantly affected by wave nonlinearity. Following the appendix in Kirby and Dalrymple (1984), we provide a heuristic extension to the mild-slope equation that is appropriate only for progressive Stokes waves. The resulting modification to (8) is given by

$$\eta_t = -\nabla_h \cdot \left(\frac{CC_g}{g}\nabla_h \tilde{\phi}\right) + \frac{(\omega^2 - k^2 CC_g + \omega C_g K'|\eta|^2)}{g}\tilde{\phi} \tag{15}$$

where

$$K' = \frac{k^3 C}{C_g}\frac{\cosh 4kh + 8 - 2\tanh^2 kh}{8\sinh^4 kh} \tag{16}$$

We apply both the linear and nonlinear model equations to the shoal described by Berkhoff et al. (1982). The data on wave amplitude was obtained over the entire vicinity of a refractive focus. The Ursell parameter remains of a reasonably small size over the entire domain of interest, thus indicating that Stokes theory should be a valid representation of the experiment.

In the model test, normally incident waves are generated at a period of $1.0s$ at the deep end of the wave tank, and are dissipated by a breaking process on a gravel beach at the shallow end. At sections 1 through 8 (see Berkhoff et al) there are arrays of resistance type wave gages spaced $0.5m$ apart which record time series of water surface elevations.

In order to dissipate wave energy at downwave boundaries, we presently use a wave damping layer at the downwave boundary. Equation (9) is modified to

$$\tilde{\phi}_t = -g\eta - w\tilde{\phi} \tag{17}$$

where

$$w = \begin{cases} 0, & x \le x_{sponge} \\ \omega\left(\frac{e^{F^n}-1}{e-1}\right), & x \ge x_{sponge} \end{cases} \tag{18}$$

4   Kirby

$$F = \frac{x - x_{sponge}}{x_{max} - x_{sponge}}, \qquad (19)$$

and the sponge length x_{sponge} is specified as 2.5 times the initial wave length.

Following a method of line approach, the model equations (8) and (17) (linear), or (15) and (17) (nonlinear) are solved using the A-B-M predictor-corrector method. The grid sizes are $\Delta x = \Delta y = 0.25m$ and $\Delta t = 1/40s$. Input wave period is $1s$. We run the models until $t = 80s$ and compute average wave heights between $t = 70s$ and $t = 80s$, after the waves reach steady state.

Referring to figure 2, where model results are compared to measured data along transects 1 through 8, we see that the linear model tends to overpredict maximum amplitudes in the vicinity of focused waves, where wave steepness may become large and nonlinear effects become important. In these regions the nonlinear models give better results. The nonlinear model results appear to contain some spurious amplitude modulations. These are not a manifestation of instability, and the effect may be suppressed by a suitable lagging of the nonlinear term in the numerical scheme.

Vincent and Briggs shoal experiment

A further study of monochromatic and random wave propagation over a shoal has been performed by Vincent and Briggs (1989). These tests are used here as a validation of the present numerical scheme as a model for irregular wave propagation.

For a random wave train, the water surface elevation may be written as

$$\eta(x, y, t) = \sum_{l=1}^{L} \sum_{m=1}^{M} A_{lm} \cos\{k_l \cos\theta_m x + k_l \sin\theta_m y - 2\pi f_l t + \psi_{lm}\} \qquad (20)$$

where A_{lm} is wave amplitude; f_l is wave frequency; θ_m is wave direction; and ψ_{lm} is random phase independent of frequency and direction. Instead of using a discrete set of wave angles, we use here a discretization of the longshore wavenumber spectrum. The longshore wavenumber λ_m is defined as

$$\lambda_m = k_l \sin\theta_m \qquad (21)$$

which determines the wave direction θ_m at each frequency. At the upwave boundary $(x = 0)$, the water surface elevation is given by
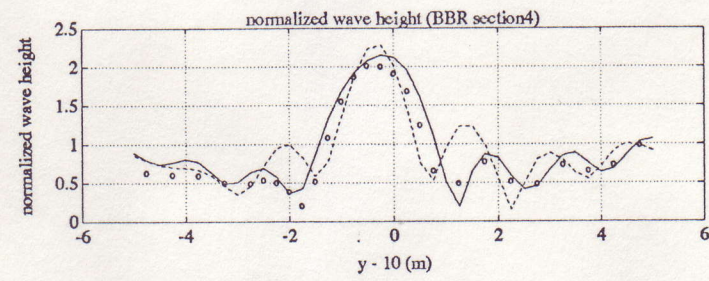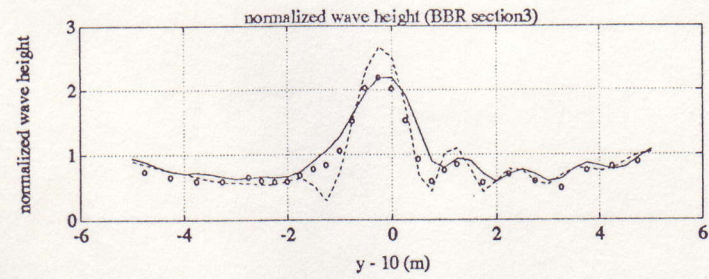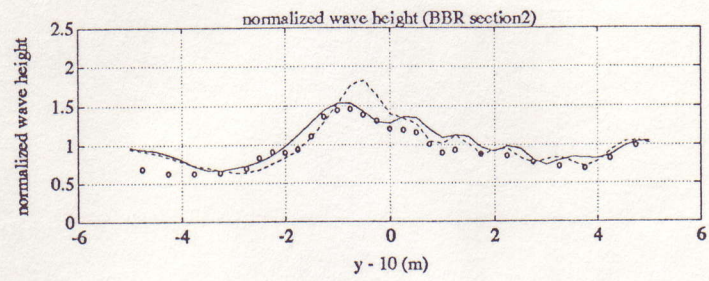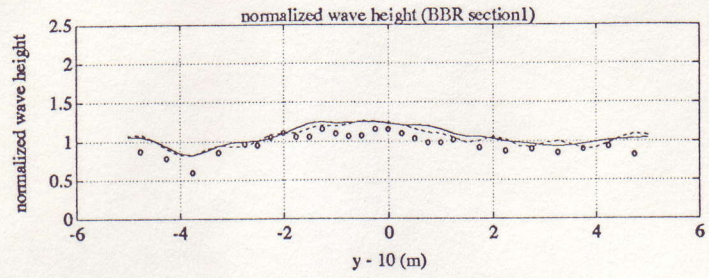
$$\eta(y, t) = \sum_{l=1}^{L} \sum_{m=1}^{M} A_{lm} \cos\{\lambda_m y - 2\pi f_l t + \psi_{lm}\} \qquad (22)$$

For given frequency f_l and longshore wavenumber λ_m, we get the amplitude of the water surface elevation

$$A_{lm} = \sqrt{2S_l(f)\Delta f \frac{S_m(\lambda)}{2\pi}\Delta\lambda} \qquad (23)$$

where $S_l(f)$ is the spectral density dependent on the frequency f and $S_m(\lambda)$ is the directional spreading function dependent on the longshore wavenumber λ. We can get $S_m(\lambda)$ from $D_m(\theta)$ (which is the spreading function dependent on the direction θ) by the condition

$$\int_{-\frac{\pi}{2}}^{\frac{\pi}{2}} D(\theta)d\theta = \int_{-k}^{k} \frac{S(\lambda)}{2\pi}d\lambda = 1, \qquad (24)$$

Kirby

5

normalized wave height (BBR section1)

normalized wave height vs y - 10 (m)

normalized wave height (BBR section2)

normalized wave height vs y - 10 (m)

normalized wave height (BBR section3)

normalized wave height vs y - 10 (m)

normalized wave height (BBR section4)
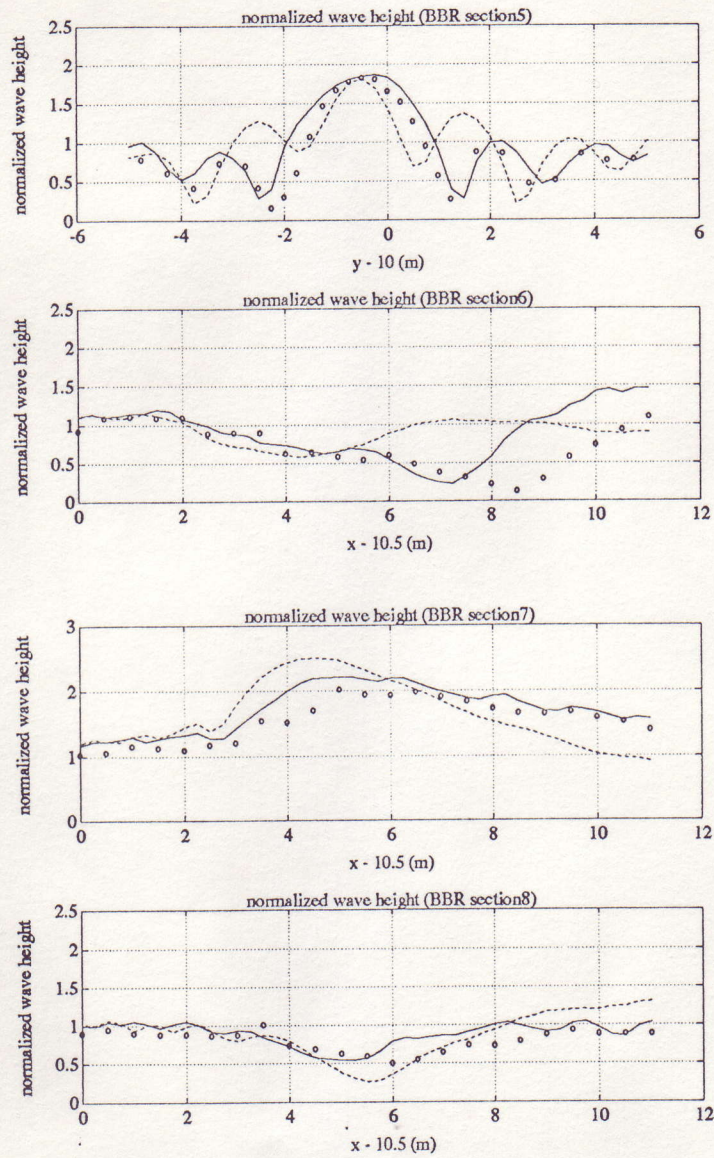
normalized wave height vs y - 10 (m)

caption on following page

Kirby

Figure 2: Comparison among linear model (dashed lines), nonlinear model (solid lines), and experimental data of Berkhoff et al. (1982)

Kirby

and so,

$$\frac{S(\lambda)}{2\pi} = D(\theta)\frac{d\theta}{d\lambda} = \frac{D(\theta)}{k\cos\theta} \qquad (25)$$

The x-component of fluid velocity at $x, z = 0$ can be obtained from the velocity potential and is given by

$$\tilde{\phi}_x = \sum_{l=1}^{L}\sum_{m=1}^{M} B_{lm}\cos\{\lambda_m y - 2\pi f_l t + \psi_{lm}\} \qquad (26)$$

where the amplitude B_{lm} is given by

$$B_{lm} = A_{lm}\frac{g\sqrt{k_l^2 - \lambda_m^2}}{2\pi f_l} \qquad (27)$$

When the spectral density $S(f)$ and the directional spreading function $D(\theta)$ are given, we can get the amplitude of the wave velocity B_{lm}. Using a 2-dimensional inverse FFT from the frequency and longshore wavenumber domain to time and y space domain, we can generate the velocity $\tilde{\phi}_x$.

Since the model equation (1) is not valid for an arbitrarily large range of frequencies, we proceed by separating the whole spectrum into several bands. In each frequency band, we then construct a wavemaker or offshore boundary condition using the spectral information falling within that band. The time-dependent mild slope equation is then solved for the narrow-banded irregular sea lying within each frequency band. The final solution is obtained by adding the different bands.

Following Vincent and Briggs (1989), we use the TMA spectrum as the target frequency spectrum and a wrapped normal function as the directional spreading function. The TMA spectrum is given by

$$S(f) = \alpha g^2 (2\pi)^{-4} f^{-5}\exp\{-1.25(\frac{f_p}{f})^4 + (\ln\gamma)\exp[-\frac{(f - f_p)^2}{2\sigma^2 f_p^2}]\}\phi(f, h) \qquad (28)$$

$S(f)$ depends on the parameters α (Phillip's constant), f_p (peak frequency) γ (peak enhancement factor) and σ (shape parameter). The factor $\phi(f, h)$ incorporates the effect of the depth h and may be approximated by

$$\phi = \begin{cases} 0.5\omega_h^2, & \omega_h < 1 \\ 1 - 0.5(2 - \omega_h)^2, & 1 \le \omega_h \le 2 \\ 1, & \omega_h > 2 \end{cases} \qquad (29)$$

where $\omega_h = 2\pi f(h/g)^{1/2}$. The parameter γ is assigned values of 2 (broad frequency) and 20 (narrow frequency). For the cases studied here, γ was assigned a value of 20. The directional spreading function $D(\theta)$ is obtained by assigning the values of either $10°$ (narrow spreading) or $30°$ (broad spreading) to the spreading parameter σ_0:

$$D(\theta) = \frac{1}{2\pi} + \frac{1}{\pi}\sum_{n=1}^{N}\exp[-\frac{(n\sigma_0)^2}{2}]\cos n(\theta - \theta_0) \qquad (30)$$

where $\theta_0 = $ mean wave direction ($= 0°$) and $N = $ number of terms in the series ($= 20$). Vincent and Briggs (1989) present a number of cases with a combination of monochromatic, narrow-banded or broad-banded frequency spectra and unidirectional, narrowbanded or broad-banded directional spreads. Here, we show results for three typical

cases: a monochromatic unidirectional sea (M2), a sea with narrow frequency and narrow directional spreading (N4), and a sea with narrow frequency and broad directional spreading (B4). All three cases involve non-breaking waves. Wave period (M2) and peak period (N4, B4) are $1.30s$. Wave height (M2) and rms wave height (N4, B4) are $2.54cm$. Phillip's α is taken to be 0.00047.

We separate the whole frequency spectrum into five components with equal band widths. The five components of the frequency spectra cover 95 percent of the total spectral density, and, using the grid spacings chosen below, the ratio of minimum wavelength to spatial grid size is 4.54. We use a weighted average of the frequencies in each frequency band to determine the representative frequency used to compute the model coefficients for each band. The band width is 0.267 Hz (see figure 3). The grid size is $\Delta x = \Delta y = 0.1905m$ and time step is $\Delta t = 1.3/80s$. We compute until $t = 260s$. Variances of water surface elevation, m_0 are computed between $t = 65s$ and $t = 260s$ and, by the assumption of the Rayleigh distribution of the wave height, significant wave heights are computed according to

$$H_s = 4\sqrt{m_0} \tag{31}$$

In figures 4-6, the water surface elevations in the whole spatial domain at $t = 260s$ are shown for cases M2, N4, and B4. The figure for Case M2 shows that the waves are long-crested and symmetric along the line crossing the center of the shoal parrallel to x axis. After the waves pass the shoal they become short-crested because of refractive focusing. When we compare the cases with directional spreading (N4 and B4) we clearly see that the wave field with broad directional spreading (B4) is more short-crested than the wave field with narrow directional spreading (N4).

In figure 7, the computed normalized wave heights along the section 4 are compared with measured data for cases M2, N4, and B4. For case M2, the normalized wave height near the centerline is greater than 2, which shows the considerable effects of refractive focusing over the shoal. For case N4, the computed results show underestimation near the centerline and overestimation away from the centerline. For case B4, the computed results show overestimation all along the section. The model results and data indicate that increasing directional spreading leads to much less spatial wave height variation induced by localized topographic irregularities. This result is seen in all spectral wave studies, and is a manifestation of the fact that the local minimums and maximums in the diffraction pattern for each spectral component overlap and experience mostly destructive interference.

Roughly, all three cases show that the model yields reasonably accurate results compared with the measured data. It is found that for directionally broad spreading case (B4) the refractive focussing effects are not noticeable behind the shoal.

Forced long waves

The forcing of long waves at difference frequencies is of particular interest in coastal design due to the influence of long waves in low frequency harbor seiching and forces on moored ships. Kirby (1983) extended the linear mild-slope equation to include forced low-frequency components, using the Stokes expansion to second order in the Lagrangian. The model for the additional low-frequency components is given by forced long wave equations, which for variable depth are given by
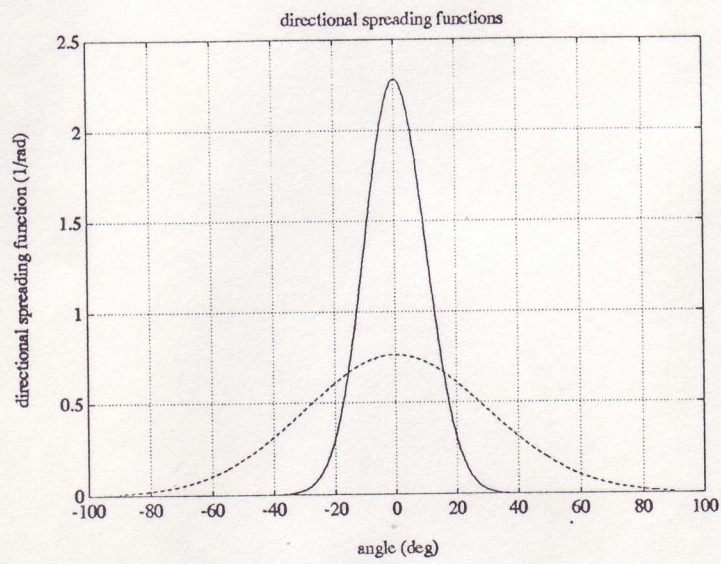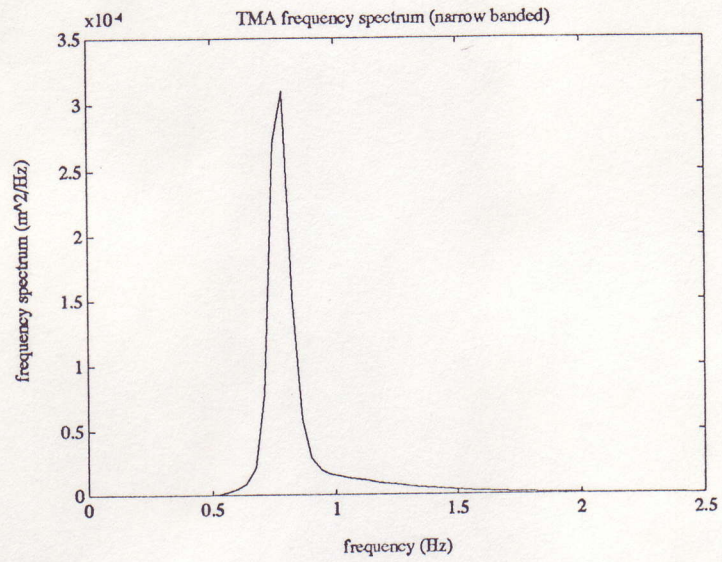
Kirby

Figure 3: TMA frequency spectra (narrow frequency band) and directional spreading functions (solid lines : $\sigma_0 = 10°$, dashed lines : $\sigma_0 = 30°$)
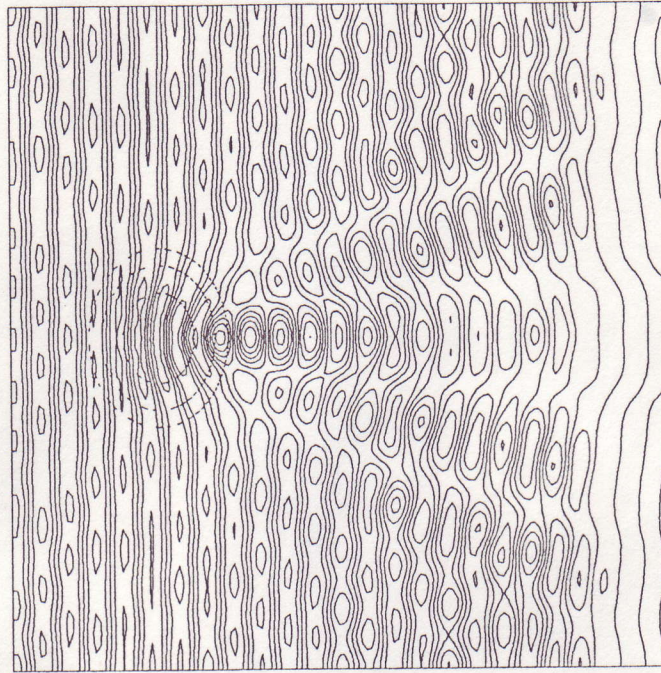
Kirby

CONTOUR FROM 0510000 TO 0540000 CONTOUR INTERVAL OF 0.50000 PT(3,3)= 0.05720

Figure 4: Water surface elevations at t = 260 seconds (case M2)

CONTOUR FROM 0510000 TO 0540000 CONTOUR INTERVAL OF 0.50000 PT(3,3)= 0.03920
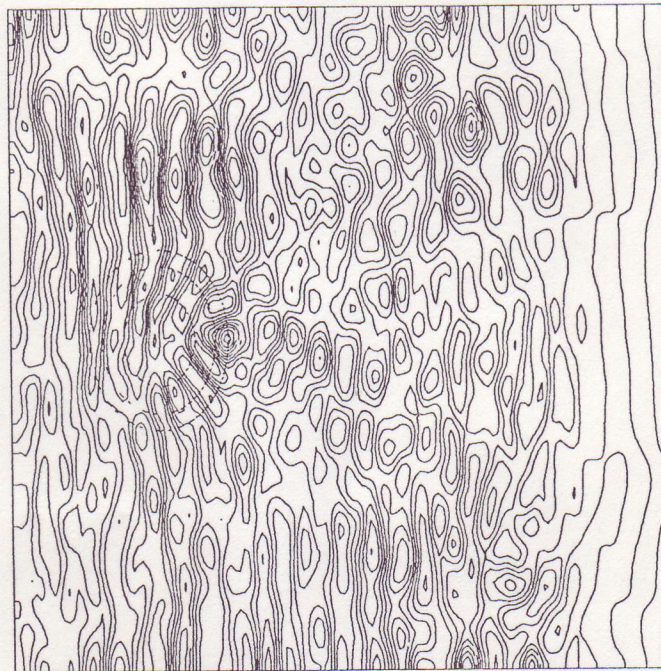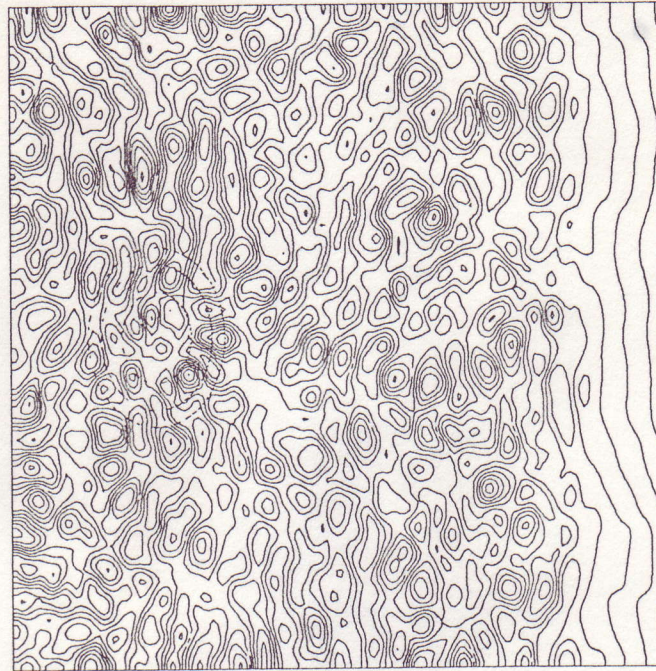
Figure 5: Water surface elevations at t = 260 seconds (case N4)

Kirby

CONTOUR FROM 0510000   TO 0540000   CONTOUR INTERVAL OF 0.50000   PT(3,3)= 0.00020

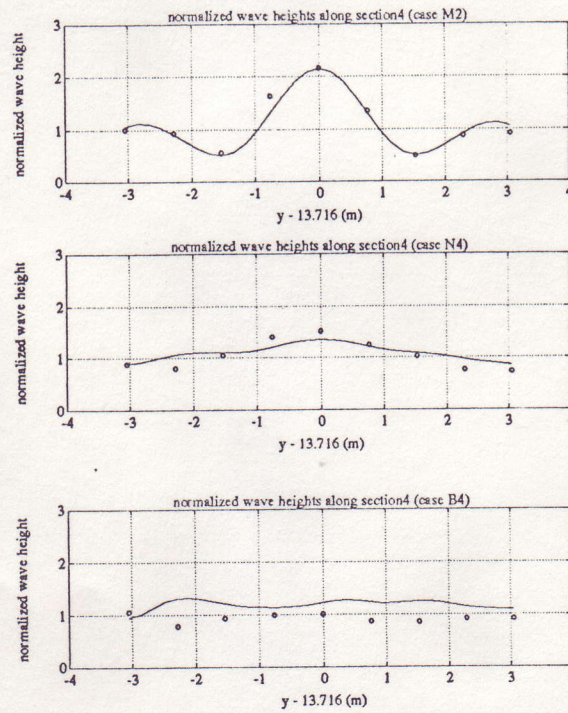Figure 6: Water surface elevations at t = 260 seconds (case B4)

Figure 7: Measured and predicted normalized wave heights on section 4

$$\eta_{2,t} + \nabla_h \cdot \{h\nabla_h\phi_2\} = -\nabla_h \cdot \{\overline{\eta\nabla_h\tilde{\phi}}\} \tag{32}$$

$$\phi_{2,t} + g\eta_2 = \frac{\omega^2}{g^2}\overline{(\tilde{\phi}_t)^2} - \frac{1}{2}\overline{(\nabla_h\tilde{\phi})^2} - \frac{\omega^4}{2g^2}\overline{\tilde{\phi}^2} \tag{33}$$

where $\overline{()}$ denotes a time average. The correct method for computing time averages in an unsteady wave train is unclear. If the wave train is narrow-banded, we may use the extraction of the dominant frequency in section 2 as the basis for isolating the slowly-varying amplitudes. Following this strategy, (32) and (33) may be further reduced to

$$\eta_{2,t} + \nabla_h \cdot \{h\nabla_h\phi_2\} = -\frac{1}{2}\mathrm{Re}\left(\nabla_h \cdot [\hat{\eta}^*\nabla_h\hat{\phi}]\right) \tag{34}$$

$$\phi_{2,t} + g\eta_2 = \frac{\omega^2}{2}\hat{\eta}\hat{\eta}^* - \frac{1}{4}\left(\nabla_h\hat{\phi} \cdot \nabla_h\hat{\phi}^*\right) - \frac{\omega^4}{4g^2}\hat{\phi}\hat{\phi}^* \tag{35}$$

These equations may also be written as a single second-order equation, analogous to (13), after elimination of η_2. The numerical schemes are again identical to those used for the basic linear equations.

Figure 8 shows a plot illustrating the generation of a single wave group and the associated bound and free long waves in a one-dimensional wave flume. The wavemaker motion used does not compensate for the decrease in total volume (at second order) associated with the entrance of the wave group into the wave channel. There is thus a free long wave generated whose net positive volume compensates for the negative volume associated with the setdown under the wave group. This positive wave propagates away from the wavemaker as a free wave, and thus leads the short wave group in the tank.

Additional results for long wave generation and harbor resonance in 2-D will be reported separately.

Conclusions

We have developed models for the numerical solution of time-dependent mild-slope equations, and applied the models to the study of irregular and regular wave propagation in the coastal environment. Linear and nonlinear versions of the mode were applied to Berkhoff shoal, and, as expected, we found that the nonlinear model showed better results than the linear model. We also applied the linear version of the model to study irregular wave refraction and diffraction by a submerged shoal, and compared model results to experimental data given by Vincent and Briggs (1989). Finally, the models were extended to include additional low frequency components which are forced by the primary wave envelopes, and some preliminary results on long wave generation were shown.

References

Berkhoff, J. C. W., 1972, "Computation of combined refraction-diffraction", *Proc. 13th Intl. Conf, Coast. Engineering*, Vancouver, 471-490.

Berkhoff, J. C. W., Booij, N., and Radder, A. C., 1982, "Verification of numerical wave propagation models for simple harmonic linear waves", *Coastal Engineering*, 6, 255-279.

Copeland, G. J. M., 1985, "A practical alternative to the 'mild-slope' wave equation", *Coastal Engineering*, 9, 125-149.

Kirby
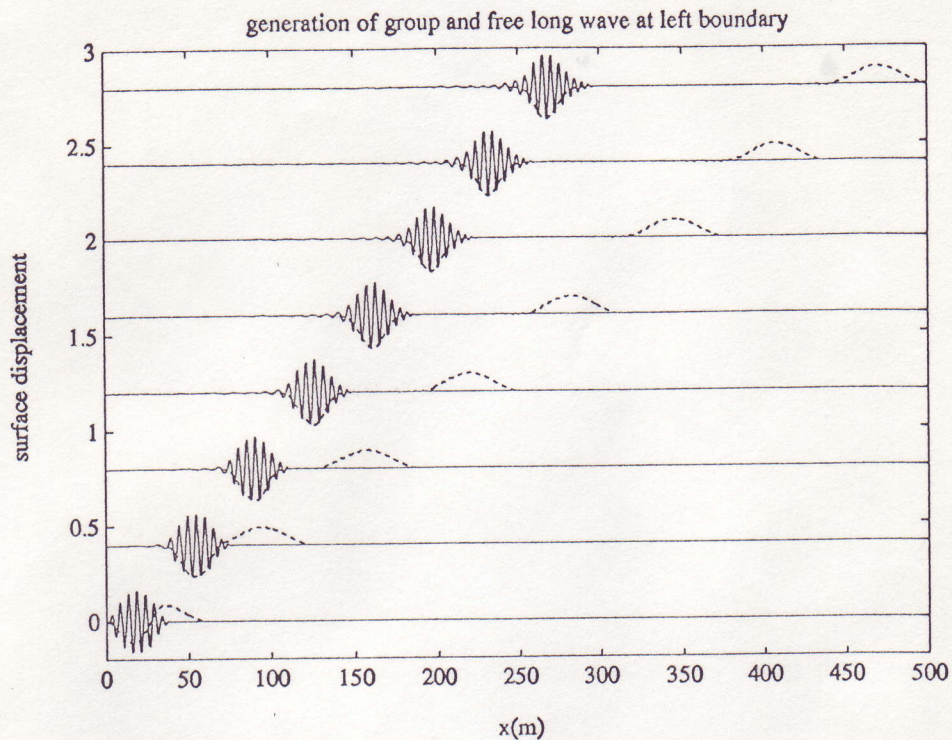
Figure 8: Generation of bound and free long waves during wave group generation.

Ito, Y. and Tanimoto, K., 1972, "A method of numerical analysis of wave propagation - application to wave diffraction and refraction", *Proc. 13th Intl. Conf. Coast. Engineering*, Vancouver, Chapt. 26.

Kirby, J. T., 1983, "Propagation of weakly-nonlinear surface water waves in regions with varying depth and current", Ph.D. thesis, University of Delaware.

Kirby, J. T. and Dalrymple, R. A., 1984, "Verification of a parabolic equation for propagation of weakly-nonlinear waves", *Coastal Engineering*, 8, 219-232.

Kirby, J. T. and Rasmussen, C., 1991, "Numerical solutions for transient and nearly periodic waves in shallow water", *Proc. ASCE Engineering Mechanics Specialty Conference: Mechanics Computing in the 1990's and Beyond*, Columbus, 328-332, May.

Madsen, P. A. and Larsen, J., 1987, "An efficient finite-difference approach to the mild-slope equation", *Coastal Engineering*, 11, 329-351.

Panchang, V. G., Pearce, B. R., Wei, G. and Cushman-Roisin, B., 1991, "Solution of the mild-slope wave problem by iteration", *Applied Ocean Res.*, 13, 187-199.

Smith, R. and Sprinks, T., 1975, "Scattering of surface waves by a conical island", *J. Fluid Mech.*, 72, 373-384.

Vincent, C. L. and Briggs, M. J., 1989, "Refraction and diffraction of irregular waves over a mound", *J. of Waterway, Port, Coastal, and Ocean Engineering*, 115, 269-284.